RSC Advances

ROYAL SOCIETY OF CHEMISTRY

www.rsc.org/advances

Graphical Abstract

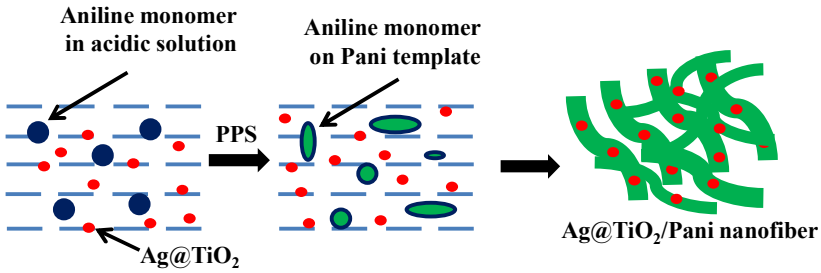

Synthesis of $Ag@TiO_2$/Pani nanocomposite by biogenic-chemical route

Journal Name

RSC Publishing

ARTICLE

Enhanced thermoelectric behaviour and visible light activity of Ag@TiO_2/Polyaniline nanocomposite synthesized by biogenic-chemical route†

Cite this: DOI: 10.1039/x0xx00000x

Received 00th January 2012,
Accepted 00th January 2012

DOI: 10.1039/x0xx00000x

www.rsc.org/

Mohd Omaish Ansari, Mohammad Mansoob Khan, Sajid Ali Ansari, Jintae Lee and Moo Hwan Cho*

This paper reports the synthesis of visible light-active Ag@TiO_2/Pani nanocomposite through a facile biogenic-chemical route. Ag@TiO_2/Pani nanocomposite was prepared by the in-situ oxidative polymerization of aniline in the presence of Ag@TiO_2 nanocomposite, which was obtained via a biogenic route. The synthesized Ag@TiO_2/Pani nanocomposite was confirmed by UV-visible spectroscopy, photoluminescence spectroscopy, transmission electron microscopy, X-ray diffraction, X-ray photoelectron spectroscopy and thermogravimetric analysis. The Ag@TiO_2/Pani nanocomposite was doped with HCl or para-toluene sulfonic acid to render it conducting. An analysis of the thermoelectrical behavior using a cyclic aging technique showed that the electrical conductivity and thermal stability of Pani got improved after incorporation of Ag@TiO_2 to form Ag@TiO_2/Pani nanocomposite system. Photocatalytic studies of the Ag@TiO_2/Pani nanocomposite revealed superior photodegradation properties in comparison to Pani towards the degradation of methylene blue and brilliant blue under visible light, even after repeated use. Electrochemical impedance spectroscopy and linear sweep voltammetry under dark and visible light irradiation also supported the visible light photocatalytic activity of Ag@TiO_2/Pani due to a decrease in the electron transfer resistance resulting in an increase in photocurrent. Therefore, the enhanced thermoelectric, photoelectrochemical and photodegradation properties of these materials suggest them to be a suitable replacement for Pani in the near future.

Introduction

In recent decades, the strong drive for industrialization has strongly affected the balance of nature, which ultimately impacts all life on Earth. A huge amount of toxic waste is released into the water streams, which not only pollutes the biosphere but also leads to bioaccumulation inside living beings. Synthetic dyes are used in many industrial fields, such as textiles, tanning, cosmetics, paper etc.[1,2] The rapid increase in the applications of synthetic dyes has led to the accumulation of their wastes in the waste water, causing severe human health problems.[3] Several methodologies, such as adsorption on inorganic or organic materials,[4,5] photocatalysis by oxidation processes,[6,7] microbiological or enzymatic decomposition,[8] have been applied for the removal of synthetic dyes from waste water. Recently, metal oxide-assisted photocatalysis has attracted considerable attention in heterogeneous catalysis.[9]

Among the many semiconducting metal oxides, TiO_2 has been the most promising and well-studied for its photocatalytic properties owing to its wide band gap, high chemical stability, large surface area, non-toxicity, and wide commercial availability.[7,10,11] The wide band gap (3.2 eV) of TiO_2, however, limits its utilization under visible light irradiation. These problems, however, can be resolved by doping TiO_2 with noble metals, such as Ag or Au to form Au or Ag@TiO_2 photocatalysts, which can be an efficient way of achieving the visible light-driven photocatalysis of TiO_2. Noble metals themselves show enhanced photocatalytic activity by absorbing visible light owing to their surface plasmon resonance and they can also work as an electron trap to activate the reaction sites.[12]

Heterogeneous-conducting polymer composites have attracted considerable attention over the past few years. Among the different conducting polymers generally used for this purpose, polyaniline (Pani), has been studied extensively because of its controllable electrical conductivity, environmental stability, good redox reversibility, and low cost.[13-16] Wang et al.[17] reported that nanocomposites of Pani with TiO_2 exhibit superior photocatalytic properties towards the degradation of methylene blue (MB) compared to TiO_2. Pani can sensitize TiO_2 by absorbing both ultraviolet and visible light, that is in contrast to pure TiO_2, which only absorbs ultraviolet light.[18]

Therefore, if Ag@TiO_2/Pani and Pani are irradiated by natural light, the former might exhibit superior visible light photocatalytic activity. Thus, in this study, Ag@TiO_2/Pani nanocomposite was

synthesized by the in-situ oxidative polymerization of aniline in the presence of Ag-modified TiO_2. The prepared nanocomposite was used for the degradation of MB and brilliant blue (BB) dyes, and was examined by electrochemical impedance spectroscopy (EIS) and linear sweep voltammetry (LSV) under visible light irradiation. The electrical conductivity and electrical stability of the materials were also evaluated; the nanocomposite showed better stability than Pani.

Experimental

Materials

Aniline, silver nitrate ($AgNO_3$, 99%), para-toluene sulfonic acid (*p*TSA, 98.5%), methylene blue (MB), brilliant blue (BB), and TiO_2 (mean particle size ~21 nm) were purchased from Sigma Aldrich. Potassium persulphate (PPS), HCl, NH_4OH, and methanol were purchased from Duksan pure chemicals, Korea, and used as received. De-ionized water obtained from a PURE ROUP 30 water purification system was used in these experiments.

Methods

X-ray diffraction (XRD, PANalytical, X'Pert-PRO MPD) was performed using Cu Kα radiation (λ = 0.15405 nm). The microstructures were observed by field emission transmission electron microscopy (FE-TEM, Tecnai G2 F20, FEI, U.S.A.). The UV-visible diffuse absorbance was measured using a UV-VIS-NIR spectrophotometer (VARIAN, Cary 5000 U.S.A.) Thermogravimetric analysis (TGA, Perkin Elmer, Pyris Dimond) was performed by heating the samples from 25 °C to 800 °C at a rate of 10 °C min^{-1} with a N_2 flow rate of 200 mL/min. X-ray photoelectron spectroscopy (XPS, ESCALAB 250) was performed using a monochromatized Al Kα X-ray source (hν = 1486.6 eV) with a 500 μm spot size. The photocatalytic degradation and photoelectrochemical experiments, such as electrochemical impedance spectroscopy (EIS) and linear sweep voltammetry (LSV), were conducted using a 400 W lamp with an irradiation intensity of 31.0 mW cm^{-2} (3M, USA). The EIS and LSV measurements were carried out using a potentiostat (Versa STAT 3, Princeton Research, USA) with a standard three-electrode system, in which Ag/AgCl (saturated with KCl), a Pt gauge and Pani or Ag@TiO_2/Pani were used as the reference, counter and working electrodes, respectively, in a 0.2 M Na_2SO_4 solution as the electrolyte.

All DC electrical conductivity (σ) measurements were performed using a 4-in-line probe electrical conductivity measuring instrument with a PID controlled oven (Scientific Equipments, Roorkee, India). The calculations were performed using the following equation:

$$\sigma = [\ln 2(2S/W)]/[2\pi S(V/I)] \quad (1)$$

where I, V, W, and S are the current (A), voltage (V), thickness of the pellet (cm), and probe spacing (cm), respectively, and σ is the DC electrical conductivity (S/cm).[19]

Synthesis of Ag@TiO_2/Pani nanocomposite

The synthesis of the Ag@TiO_2/Pani nanocomposite was carried out in two steps: the synthesis of Ag@TiO_2, followed by its incorporation with Pani to prepare Ag@TiO_2/Pani nanocomposite. The synthesis of Ag@TiO_2 can be observed elsewhere.[20] The nanocomposite of Ag@TiO_2/Pani was prepared by the in-situ rapid oxidative polymerization of aniline in the presence of the Ag@TiO_2 nanocomposite. First, the Ag@TiO_2 nanocomposite (0.03 g) was dispersed in 200 mL of a 1 M HCl solution and ultrasonicated for 5 min. Aniline (1 mL) was added dropwise to the above dispersion of Ag@TiO_2 with vigorous stirring to allow the optimal adsorption of aniline monomers on the Ag@TiO_2 nanocomposite. Subsequently, the solution of PPS (made in 1 M HCl) was added quickly to the above solution to polymerize the aniline adsorbed on Ag@TiO_2. The resulting mixture turned slowly to greenish black colored slurry, which was filtered, washed thoroughly with double distilled water, followed by dedoping with ammonia solution and then again washing with excess of water and methanol to remove any adhering trace of PPS or other impurities. The wet product after washing was doped with acid (HCl or *p*TSA) by stirring in 200 mL of 1M acid solution for 2 h, followed by filtering. The product was dried at 60 °C for 24 h and a fine powder of the nanocomposite was obtained by grinding the material using a mortar and pestle.

Studies and measurements

The electrical conductivity of Pani and Ag@TiO_2/Pani nanocomposite was measured using pelletized samples on a hydraulic pressure instrument at a 50 kN pressure for 10 min. The stability of the Ag@TiO_2/Pani nanocomposite was examined in terms of their retention of DC electrical conductivity under cyclic aging conditions. In the cyclic aging experiments, the DC electrical conductivity was measured at temperatures ranging from 40 to 150 °C for five times at 45 min intervals.

The Ag@TiO_2/Pani nanocomposite was also tested for the photocatalytic degradation of MB and BB under visible light irradiation; details of the experimental setup are reported elsewhere.[20,21] Details of the photoelectrochemical measurements, such as EIS and LSV, can be obtained from previous reports.[6,7]

Results and discussion

Proposed synthesis mechanism

The Ag@TiO_2 nanocomposite was synthesized by a biogenic route, as reported elsewhere.[20,22] The Pani and Ag@TiO_2/Pani nanocomposite were prepared using an *in-situ* rapid oxidative polymerization technique later doping them with different acids (HCl and *p*TSA) to make them conducting. The protons and counter ion of the doping acids affect the redox properties of the Pani. The doping phenomenon is governed by the principle of charge electroneutrality and the incorporation of positive charges on the Pani backbone (p-type doping due to the incorporation of proton), whereas the negative counter ion remained as the oxidation state of the polymer was changed. Therefore depending on the degree of protonation and the nature of the counter ion, doping with different

acids would lead to Pani or Ag@TiO_2/Pani with different redox properties.[23]

In the case of rapid oxidative polymerization of aniline the oxidant is added quickly to the acidic solution of aniline resulting in rapid polymerization. This polymerization technique results in fibrous morphology of aniline. The formation of one dimensional structure can be explained on the theory of rapid mixing of acidic solution of oxidant with the acidic solution of aniline monomer. As soon as the oxidant solution is mixed, the polymerization of aniline takes place and this small chain of Pani acts as template on which adsorption of aniline monomer and their subsequent polymerization occurs. Thus, in this case of rapid mixing method, the PPS is consumed at the onset of polymerization; hence secondary growth of Pani is limited resulting in the formation of nanofibers. The schematic diagram for the synthesis of Pani or Ag@TiO_2/Pani nanocomposite is given in Fig. 1.

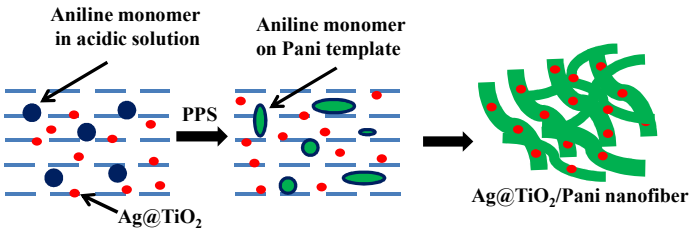

Fig. 1. Schematic diagram for the synthesis of Ag@TiO_2/Pani nanocomposite.

X-ray diffraction

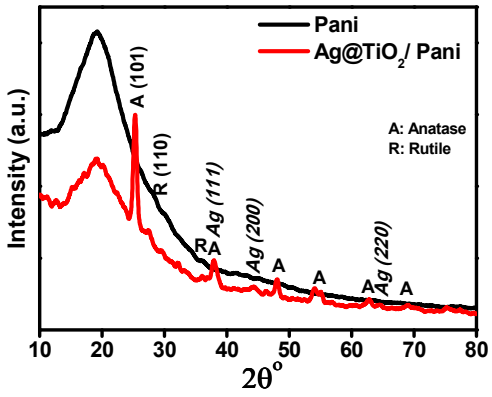

Fig. 2. XRD patterns of Pani and Ag@TiO_2/Pani nanocomposite.

Fig. 2 shows XRD patterns of Pani and the Ag@TiO_2/Pani nanocomposite. In the case of Pani, a broad peak at 19.51° 2θ was assigned to the periodicity parallel to the polymer chain.[13] The XRD pattern of Ag@TiO_2/Pani showed all the diffraction peaks corresponding to the anatase and rutile phase of TiO_2, as reported in previous work.[20] The XRD peaks corresponding to TiO_2 and Ag matched with tetragonal and face-centered cubic structures, respectively. These results suggest that TiO_2 and Ag are present as two different and distinct materials with no inter-diffusion. The XRD patterns of anatase TiO_2 nanoparticles were similar to that reported in the JCPDS file No. 73-1764. The rutile phase appeared in the XRD peaks, which was confirmed by the JCPDS file No. 76–318. All the peaks of Ag were assigned to the diffraction of the planes of face-centered cubic Ag (JCPDS file No. 04-0783). On the other hand, the peaks for Ag were diffused, which might be due to its low content and small particle size in the nanocomposite system. Other studies also reported missing or diffused XRD peaks due to the low concentration of the nanomaterial in their nanocomposite system.[24-28]

Optical Properties

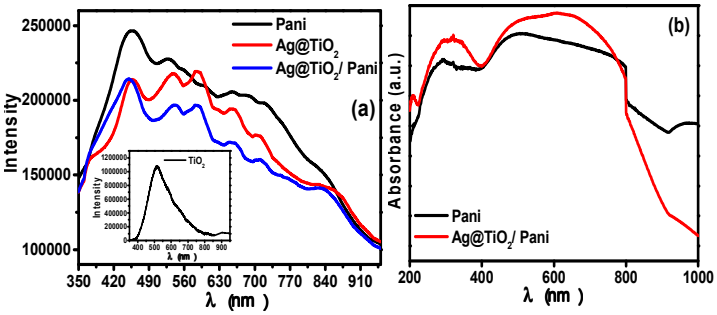

Fig. 3. (a) PL spectra of Pani, Ag@TiO_2 and Ag@TiO_2/Pani nanocomposite (Pure TiO_2 in inset), and **(b)** UV-vis diffuse absorbance spectra of Pani and Ag@TiO_2/Pani nanocomposite.

Fig. 3a shows the PL emission spectra of TiO_2, Ag@TiO_2, Pani and Ag@TiO_2/Pani nanocomposite. PL was carried out to determine the charge recombination and migration efficiency of Ag@TiO_2 and Ag@TiO_2/Pani because the photocatalytic activity is proportional to the PL intensity and the recombination rate of the photo-excited electrons and holes. The higher PL intensity of TiO_2 in comparison to Ag@TiO_2 and Ag@TiO_2/Pani shows its much lower photocatalytic activity. The excitation wavelength for both Ag@TiO_2 and Ag@TiO_2/Pani falls within the visible light region, showing that both Ag@TiO_2 and Ag@TiO_2/Pani are visible light active. The peaks from 450-500 nm were attributed to the recombination of free electrons from the conduction band to the recombination center at the ground state. In the case of Ag@TiO_2/Pani, the emission peak at ~450 nm showed comparable intensity, whereas the peak at ~540 nm had lower intensity, indicating a slightly lower recombination rate of electrons than Ag@TiO_2. A lower PL intensity means a lower electron-hole recombination rate; hence the photogenerated carriers have a longer lifetime. This suggests that the photo-induced electrons and holes were trapped by the synergy between the Ag 3d energy level and Pani, which suppresses the automatic recombination process of photogenerated electrons and holes in Ag@TiO_2/Pani compared to TiO_2 and Ag@TiO_2. In general, the efficient charge separation and inhibited electron-hole recombination of Ag@TiO_2/Pani are favorable for enhancing its photocatalytic activity. Thus from the PL spectra it can be concluded that anchoring Ag@TiO_2 could effectively inhibit the recombination of electrons and holes during the photocatalytic reaction under visible light irradiation.

Fig. 3b shows the UV-vis diffuse absorbance spectra of Pani and Ag@TiO_2/Pani nanocomposite. The spectra in the case of Pani as well as Ag@TiO_2/Pani are dominated by two peaks at ~280 and ~550 nm, which is a characteristic of Pani. The band at 280 nm was assigned to a π-π transition in the benzenoid structure, whereas the absorption in the visible range at ~550 nm was ascribed to exciton formation in the quinoid rings.[29] In the case of Ag@TiO_2/Pani, the peaks were red shifted, indicating the coordination of Ag@TiO_2 with a nitrogen atom, and a permitted interaction with each other via the π-conjugated system was observed. The red shift upon the addition of Ag@TiO_2 was consistent with a previous report in the case of Pani nanocomposite.[30] The increase in the absorption intensity after the incorporation of Ag@TiO_2 can be related to the better visible light activity of Ag@TiO_2/Pani. Fig. S1 shows the UV-vis diffuse absorbance spectra of TiO_2 and Ag@TiO_2/Pani nanocomposite. From the figure it can be seen that TiO_2 does not possess absorbance in the visible light region while in contrast Ag@TiO_2/Pani nanocomposite shows high visible light absorbance which accounts for its high visible light photoactivity.

XPS analysis

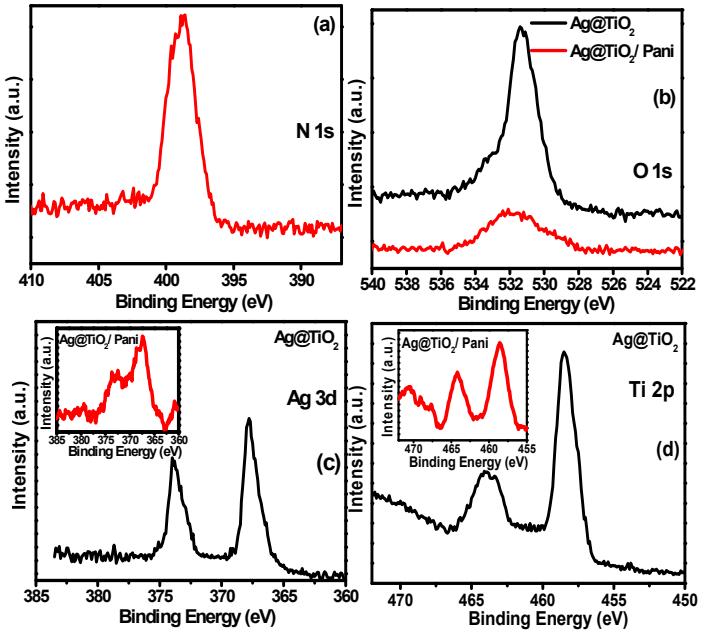

Fig. 4. XP spectra of the Ag@TiO_2 and Ag@TiO_2/Pani nanocomposite for **(a)** N 1s peaks, **(b)** O 1s peaks, **(c)** Ag 3d peaks (inset shows Ag 3d of Ag@TiO_2/Pani), and **(d)** Ti 2p peaks (inset shows Ti 2p of Ag@TiO_2/Pani).

XPS was performed to analyze the chemical composition of the Ag@TiO_2 and Ag@TiO_2/Pani nanocomposite. The survey spectra revealed C, Ag, O and Ti in Ag@TiO_2, as well as N in Ag@TiO_2/Pani corresponding to the nitrogen in the Pani backbone (Fig. S2). The residual carbon from the sample and hydrocarbons from XPS are depicted from peak in Fig. S3 (284.6 eV). The N 1s peak at 398.75 eV in Fig. 4a can be assigned to the positively-charged quinoid amine and benzenoid amine, which is consistent with previous work.[31] In the O 1s spectra of Ag@TiO_2 and Ag@TiO_2/Pani (Fig. 4b), the peaks were assigned to O bonding, such as Ti-O-Ti and Ti-O-H.[32] Chen et al.[33] stated that the surface oxidation of Pani, or weakly charge-transfer-complexed oxygen atoms can make another contribution to the O 1s spectra in the case of Ag@TiO_2/Pani. The shift in the binding energy of O 1s in the case of Ag@TiO_2 and Ag@TiO_2/Pani from 531.30 to 531.79 eV, respectively, can be attributed to the strong interactions between the oxygen of TiO_2 and the imine nitrogen.

Fig. 4c shows the Ag 3d spectra of the Ag@TiO_2 (367.73 eV) and Ag@TiO_2/Pani (367.71) nanocomposite, whereas Fig. 4d presents the Ti 2p spectra of Ag@TiO_2 (458.39 eV) and Ag@TiO_2/Pani (458.70 eV) nanocomposite. In the case of Ag@TiO_2/Pani, the signals of Ag 3d (inset of Fig. 4c) and Ti 2p (inset of Fig. 4d) are very weak, which may be due to the surface coating of Pani over Ag@TiO_2 during the polymerization process.

TEM analysis

TEM was conducted to examine the inner nanostructure of the as-prepared Ag@TiO_2/Pani nanocomposite. Fig. 5a shows a typical TEM image of the Ag@TiO_2/Pani nanocomposite. Pani largely possessed a tubular morphology with a scattered Ag@TiO_2 nanocomposite. As shown in Fig. 5b, the length of tubular Pani was approximately 100-200 nm, and the mean diameter was ~40 nm. Some nanoparticles with a mean size of 10 nm were observed on the surface of the Pani tubule, which were indexed to the Ag@TiO_2 nanocomposite. The fibrous nature of Pani can be seen clearly from the images (additional images are shown in Fig. S4). In addition, the fibrous nature of Pani imparted significant porosity to the Ag@TiO_2 nanocomposite, which is also an important factor for the synergistic effect. The SAED pattern of nanocomposite (Fig. S5) has a distinct diffraction maximum and the sequential appearance of dark and bright fringes, which are characteristic of polycrystalline structures.

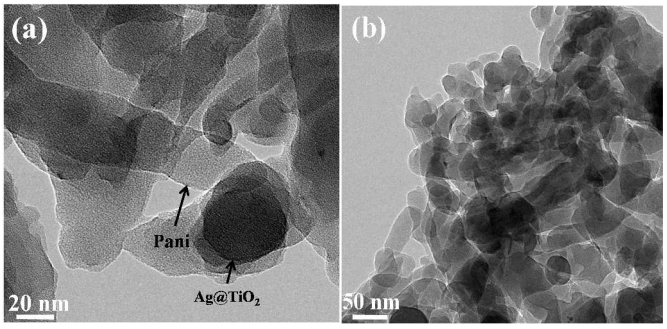

Fig. 5. TEM images of the as-prepared Ag@TiO_2/Pani nanocomposite at different magnifications (a and b).

Thermogravimetric analysis

The thermal stability of the nanocomposite and the interactions between Ag@TiO_2 and Pani were examined by TGA. Fig. 6 shows the thermograms of Pani and the Ag@TiO_2/Pani nanocomposite.

Pani and the Ag@TiO_2/Pani nanocomposite showed distinct steps of thermal degradation. The first weight loss up to ~100 °C was assigned to the evaporation of free water molecules and other volatile impurities. Wang et al.[34] also reported a similar trend for ferrite-grafted Pani nanofibers. The weight loss from ~100 to 400 °C was attributed to the removal of water and dopant molecules adsorbed on Pani, and to the degradation of oligomers. The third degradation step was assigned to decomposition of the molecular chains of Pani. The degradation of the Pani backbone from ~400 °C to 550 °C resulted in the formation of aliphatic and aromatic fragments, such as ammonia, aniline, p-phenylenediamine, N-phenylaniline, N-phenyl-1,4-benzenediamine, carbazole, pyridine based heterocycle, methane, acetylene, etc.[35] As expected, the Ag@TiO_2/Pani nanocomposite became more resistant to thermal degradation, possibly due to the strong interactions between the Ag@TiO_2 and Pani surface. A similar trend of increased thermal stability after the incorporation of nanoparticles was also reported by Liu et al.[36] in their study of graphene@Pani nanofibers composites.

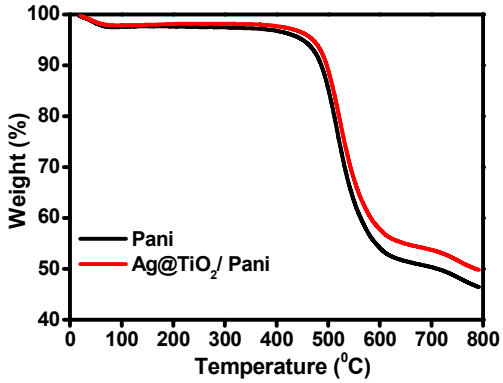

Fig. 6. TGA of Pani and Ag@TiO_2/Pani nanocomposite.

Electrical conductivity

The measured DC electrical conductivity of the HCl doped Pani and Ag@TiO_2/Pani were 5.55 and 6.14 S/cm, respectively, whereas the conductivity of *p*TSA doped Pani and Ag@TiO_2/Pani were 12.28 and 14.8 S/cm, respectively. The electrical conductivity of Pani was found to be dependent on the type of doping acids used and the Ag@TiO_2 inside the nanocomposite. The higher electrical conductivity in the case of the *p*TSA doped samples may be due to an increase in the metallic regions in the nanocomposite, a decrease in the hopping/tunneling distance, and an increase in the density of charge carriers.[14,15] The DC electrical conductivity of Ag@TiO_2 nanocomposite was measured to be 27.5 S/cm. The increase in the electrical conductivity after the incorporation of Ag@TiO_2 in Pani in both cases (i.e. in the case of HCl and *p*TSA doped samples) can be attributed to the additional/synergistic effect of both Pani and Ag@TiO_2, which leads to an increase in conductivity. In addition, the incorporation of Ag@TiO_2 is expected to form a more efficient network for charge transport.[14,15]

In the case of cyclic aging studies, the DC electrical conductivity increased with increasing temperature from 40 to 150 °C, which is normal thermal activation behavior (Table S1). Fig. 7 shows that the initial electrical conductivity at the beginning of each cycle decreases with increasing number of cycles for all samples. This may be due to the loss of moisture during cyclic aging and the degradation of Pani inside the nanocomposite system. The percentage retention of the DC electrical conductivity at the start of the fifth cycle was also calculated. HCl doped Ag@TiO_2/Pani showed ~51.5 % whereas *p*TSA doped Ag@TiO_2/Pani showed ~55.5 % DC electrical conductivity retention. The higher retention in the case of the *p*TSA doped sample might be due to the lower volatility of *p*TSA compared to HCl, suggesting the higher stability of *p*TSA doped Ag@TiO_2/Pani compared to the HCl doped Ag@TiO_2/Pani nanocomposite for practical applications.

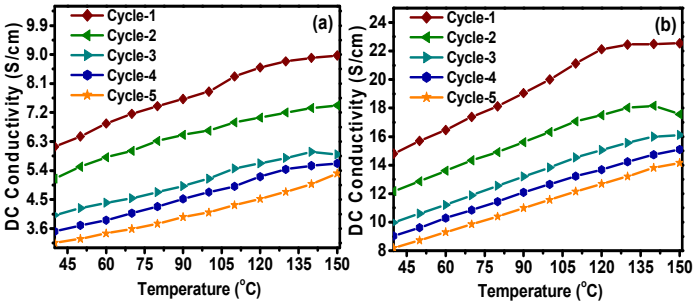

Fig. 7. DC electrical conductivity of Ag@TiO_2/Pani nanocomposite, **(a)** HCl doped and **(b)** *p*TSA doped at varying temperatures under cyclic aging conditions.

Photoelectrochemical studies

Fig. 8a shows the EIS response, which is an effective tool for probing the photogenerated charge separation and transport properties of the Pani and Ag@TiO_2/Pani nanocomposite under dark and visible light irradiation.[6,7,21,37] The arc radii of the EIS Nyquist plot of Ag@TiO_2/Pani photocatalysts were smaller than those of Pani under dark and visible light irradiation, suggesting that Ag@TiO_2/Pani photocatalysts have lower resistance than Pani, which can accelerate the interfacial charge-transfer process. This also shows that more effective separation of the photogenerated electron hole pairs and faster interfacial charge transfer occurred in the case of Ag@TiO_2/Pani nanocomposite.[6,7,21,37-43] This confirms that the Ag@TiO_2/Pani photocatalyst has the lowest charge transfer resistance and is most suitable for photocatalytic applications. These enhanced photoelectric characteristics suggest that the interfacial interaction of Ag@TiO_2 and Pani can improve the photocatalytic efficiency of Pani effectively in the Ag@TiO_2/Pani nanocomposite system.

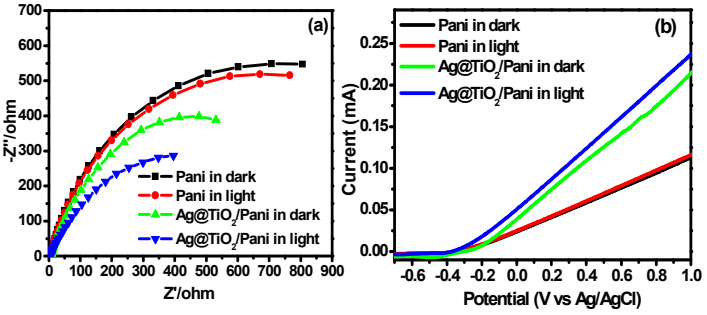

Fig. 8. (a) EIS (Nyquist plots), and (**b**) LSV spectra of Pani and the Ag@TiO_2/Pani nanocomposite under dark and visible light irradiation.

To examine the possible mechanisms for the enhanced visible light photoactivity (i.e. photocurrent), LSV for Pani and Ag@TiO_2/Pani were performed under dark and visible light irradiation. Fig. 8b shows the photoresponse of Ag@TiO_2/Pani and Pani under dark and visible light irradiation. The photocurrent of Ag@TiO_2/Pani was improved compared to Pani and Ag@TiO_2/Pani showed a higher photocurrent than Pani under the same conditions, suggesting that Ag@TiO_2/Pani had stronger ability to separate the electron-hole pairs than Pani, which is also consistent with the PL results. The significant improvement in the photocurrent for Ag@TiO_2/Pani shows that it can be motivated easily by visible light, and produce more photoinduced carriers, resulting in high visible light photocatalytic activity.[6,7,40] These results suggest that the separation efficiency of the photoinduced electrons and holes was enhanced considerably by the synergistic effects of Ag@TiO_2 and Pani.

Visible light photocatalytic activities of Pani and Ag@TiO_2/Pani

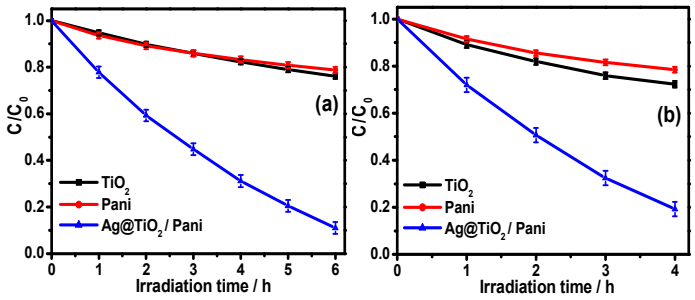

Fig. 9. Plot of C/C_0 vs. the irradiation time (h) for the photodegradation of (**a**) MB, and (**b**) BB by TiO_2, Pani and Ag@TiO_2/Pani nanocomposite.

Fig. 9a and 9b show the photocatalytic activity of TiO_2, Pani and Ag@TiO_2/Pani under visible light irradiation, indicating the photodegradation efficiency of Ag@TiO_2/Pani for the degradation of MB and BB. The performance of Ag@TiO_2/Pani was significantly higher than TiO_2 as well as Pani and the other reported nanocomposites of Pani under UV light.[44] Fig. 10 shows the mechanism for the photo generation of charge carriers on the surface of the Ag@TiO_2/Pani photocatalyst.

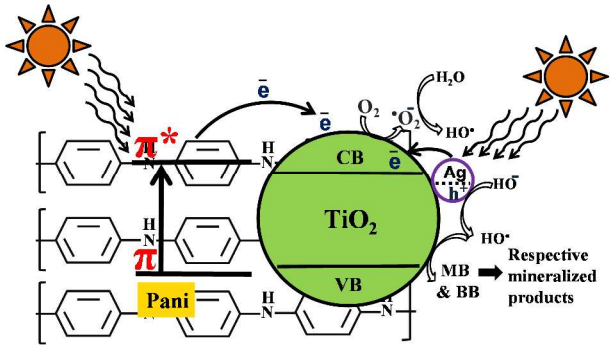

Fig. 10. Proposed mechanism for the degradation of MB and BB by the Ag@TiO_2/Pani nanocomposite.

Under visible light irradiation, Pani absorbs light to induce a $\pi \rightarrow \pi^*$ transition, transporting the excited-state electrons to the π^* orbital. These excited-state electrons can be injected readily into the conduction band of TiO_2, are subsequently transferred to the surface, and react with adsorbed water and oxygen to yield hydroxyl and superoxide radicals while holes react with HO^- to yield hydroxyl radicals.[6,7,20,41] Furthermore, during visible light irradiation, the equilibrated Fermi level electrons of Ag are injected rapidly into the TiO_2 conduction band via a surface phonon resonance (SPR) mechanism (Fig. 10).[6,19,21,37] These injected electrons are trapped by adsorbed oxygen/water molecules on Ag@TiO_2 to yield hydroxyl and superoxide radicals. Therefore, the large amounts of oxidative radical formation are responsible for the enhanced photocatalytic activity of the Ag@TiO_2/Pani photocatalyst.[6,7,37-41] Owing to the synergy between Ag@TiO_2 and Pani, the rapid photogenerated charge separation and relatively slow charge recombination enhances the photocatalytic activity of the Ag@TiO_2/Pani photocatalyst significantly.[6,38]

The photocatalytic activity of the Pani and Ag@TiO_2/Pani photocatalyst for the degradation of MB and BB was also checked under UV irradiation (Fig. S6). From the figure it can be seen that both Pani and Ag@TiO_2/Pani does not show UV light activity and thus our nanocomposite is workable only in visible light region.

The reusability of the Ag@TiO_2/Pani nanocomposite catalyst was tested by centrifuging the catalyst from the dye solution, which was followed by washing with distilled water and drying. The reused catalyst showed a similar response to that of the fresh catalyst, suggesting the applicability of the proposed method.

Conclusions

A visible light active Ag@TiO_2/Pani nanocomposite was successfully prepared using a simple biogenic-chemical route. The studies on the DC electrical conductivity showed that the electrical conductivity and the retention of DC electrical conductivity under cyclic aging conditions were dependent on the dopant acid. The nanocomposite revealed high conductivity (12.28 and 14.8 S/cm) compared to Pani (5.55 and 6.14 S/cm) because of the high mobility of charge carriers in the presence of Ag@TiO_2. The *p*TSA doped Ag@TiO_2/Pani nanocomposite studied under cyclic aging conditions showed higher retention of DC electrical conductivity compared to HCl doped Ag@TiO_2/Pani, which was attributed to the smaller loss of dopant under aging conditions. The Ag@TiO_2/Pani nanocomposite was studied for visible light decomposition of MB and BB, and showed enhanced photocatalytic activity compared to Pani. The recycling test also showed that the Ag@TiO_2/Pani nanocomposite can be used repeatedly without significant loss of visible light activity. The high photocatalytic activity can be attributed to the synergistic effect originating from the excited state electrons, which are injected readily into the conduction band of TiO_2. Their better photoelectrochemical (EIS and LSV), photocatalytic and thermoelectric performance means that more

efforts should be made to improve the performance of the Ag@TiO_2/Pani nanocomposites, widen their applications and achieve commercialization in the near future.

Acknowledgements

This study was supported by Basic Science Research Program through the National Research Foundation of Korea (NRF) funded by the Ministry of Education, Science and Technology (Grant No: 2012R1A1A4A01005951).

Notes and references

School of Chemical Engineering, Yeungnam University, Gyeongsan-si, Gyeongbuk 712-749, South Korea. Phone: +82-53-810-2517; Fax: +82-53-810-4631,
***Email:** mhcho@ynu.ac.kr*

†Electronic Supplementary Information (ESI) available: [UV-vis diffuse absorbance spectra pure TiO_2 and Ag@TiO_2/Pani, XPS survey of Ag@TiO_2 and Ag@TiO_2/Pani, C1s Ag@TiO_2 and Ag@TiO_2/Pani, TEM images of Ag@TiO_2/Pani, HR-TEM images of Ag@TiO_2/Pani, SAED patterns of Ag@TiO_2/Pani, Table S1 electrical conductivity of Ag@TiO_2/Pani and plot of C/C_0 *vs* the time for the photodegradation of MB and BB under UV light irradiation] See DOI: 10.1039/b000000x/

1 M. A. Salem, A. F. Al-Ghonemiy and A. B. Zaki, *Appl. Catal. B-Environ*., 2009, **91**, 59.
2 B. O. Regan, L. Xiaoe and T. Ghaddar, *Energy. Environ. Sci.*, 2009, **5**, 7203.
3 Priyanka and V. C. Srivastava, *Ind. Eng. Chem. Res.*, 2013, **52**, 17790.
4 R. Kumar, M. O. Ansari and M. A. Barakat, *Chem. Eng. J.*, 2013, **228**, 748.
5 R. Kumar, M. Kumar, R. Ahmad and M. A. Barakat, *Chem. Eng. J.*, 2013, **218**, 32.
6 S. A. Ansari, M. M Khan, M. O. Ansari, J. Lee and M. H. Cho, *J. Phys. Chem. C*, 2013, **117**, 27023.
7 M. M. Khan, S. A. Ansari, D. Pradhan, M. O. Ansari, D. H. Han, J. Lee and M. H. Cho, *J. Mater. Chem. A*, 2014, **2**, 637.
8 M. Solís, A. Solís, H. I. Pérez, N. Manjarrez and M. Flores, *Process Biochem.*, 2012, **47**, 1723.
9 H. Kisch, *Angew. Chem. Int. Edit*., 2013, **52**, 812.
10 C. Chen, Q. Liu, S. Gao, K. Li, H. Xu, Z. Lou, B. Huang and Y. Dai, *RSC Adv.*, 2014, **4**, 12098.
11 Q. Zhu, Y. Peng, L. Lin, C. M. Fan, G. Q. Gao, R. X. Wang and A.W. Xu, *J. Mater. Chem. A*, 2014, **2**, 4429.
12 P. Wang, B. Huang, Y. Dai and M. H. Whangbo, *Phys. Chem. Chem. Phys*., 2012,**14**, 9813.
13 M. O. Ansari, M. M. Khan, S. A. Ansari, I. Amal, J. Lee and M. H. Cho, *Mater. Lett*., 2014, **114**, 159.
14 M. O. Ansari, M. M. Khan, S. A. Ansari, I. Amal, J. Lee and M. H. Cho, *Chem. Eng. J*., 2014, **242**, 155.
15 M. O. Ansari and F. Mohammad, *Sensor Actuat. B- Chem*., 2011, **157**, 122.
16 M. O. Ansari and F. Mohammad, *Compos. Part B-Eng*., 2012, **43**, 3541.
17 F. Wang and S. X. Min, *Chin. Chem. Lett.*, 2007, **18**, 1273.
18 M. A. Salem, A. F. Al-Ghonemiy and A. B. Zaki, *Appl. Catal. B*, 2009, **91**, 59.
19 M. O. Ansari and F. Mohammad, *J. Appl. Polym. Sci*., 2012, **124**, 4433.
20 M. M. Khan, S. A. Ansari, M. I. Amal, J. Lee and M. H. Cho, *Nanoscale*, 2013, **5**, 4427.
21 S. A. Ansari, M. M. Khan, S. Kalathil, A. Nisar, J. Lee and M. H. Cho, *Nanoscale*, 2013, **5**, 9238.
22 S. Kalathil, M. M. Khan, J. Lee and M. H. Cho, *Biotechnol. Adv.*, 2013, **31**, 915–924.
23 D. W. Hatchett, M. Josowicz and J. Janata, *J. Phys. Chem. B*, 1999, **103**,10992.
24 J. J. Wang, A. F. Lv, Y. Q. Wang, B. Cui, H. J. Yan, J. S. Hu, W. P. Hu, Y. G. Guo and L. J. Wan, *Sci. Rep*., 2013, **3**, 2613.
25 Q. Zhen, R. N. Vannier and G. M. Kale, *Mater. Sci. Eng. A-Struct*., 2007, **444**, 130.
26 K. Kondoh, T. Threrujirapapong, H. Imai, J. Umeda and B. Fugetsu, *Compos. Sci. Technol*., 2009, **69**, 1077.
27 R. Pérez-Bustamante, F. Pérez-Bustamante, I. Estrada-Guel, C. R. Santillán-Rodríguez, J. A. Matutes-Aquino, J. M. Herrera-Ramírez, M. Miki-Yoshida and R. Martínez-Sánchez, *Powder Technol*., 2011, **212**, 390.
28 Y. Wu and G. Y. Kim, *J. Mater. Process. Techn.*, 2011, **211**, 1341.
29 S. Pruneanu, E. Veress, I. Marian and L. Oniciu, *J. Mater. Sci*., 1999, **34**, 2733.
30 K. Mallick, M. Witcomb and M. Scurrell, *Platinum Metals Rev.*, 2007, **51**, 3.
31 A.G. Macdiarmid, J. C. Chiang, A. F. Richter and A. J. Epstein, *Synthetic Met.*, 1987, **18**, 285.
32 F. Y. Chuang and S. M. Yang, *Synthetic Met.*, 2005, **152**, 361.
33 W. Chen, R. B. Rakhi and H. N. Alshareef *J. Mater. Chem. A*, 2013, **1**, 3315.
34 W. Wang, S. P. Gumfekar, Q. Jiao and B. Zhao, *J. Mater. Chem. C*, 2013, **1**, 2851.
35 M. O. Ansari and F. Mohammad, *Compos. Part B- Eng*., 2012, **43**, 3541.
36 S. Liu, X. Liu, Z. Li, S. Yang and J. Wang, *New J. Chem.*, 2011, **35**, 369.
37 S. A. Ansari, M. M. Khan, M. Omaish, J. Lee and M. H. Cho, *New J. Chem.*, 2014, DOI: 10.1039/C3NJ01488F.
38 S. A. Ansari, M. M. Khan, J. Lee and M. H. Cho, *J. Ind. Eng. Chem*., 2014, http://dx.doi.org/10.1016/j.jiec.2013.08.006.
39 X. Bai, L. Wang, R. Zong, Y. Lv, Y. Sun and Y. Zhu, *Langmuir*, 2013, **29**, 3097.
40 J. Gan, X. Lu, J. Wu, S. Xie, T. Zhai, M. Yu, Z. Zhang, Y. Mao, S. C. Wang, Y. Shen and Y. Tong, *Sci. Rep.*, 2013, **3**, 1021.
41 W. H. Leng, Z. Zhang, J. Q. Zhang and C. N. Cao, *J. Phys. Chem. B*, 2005, **109**, 15008.
42 S. A. Ansari, M. M. Khan, M. Omaish, J. Lee and M. H. Cho, *RSC Adv.*, 2014, **4**, 16782.
43 M. M. Khan, S. A. Ansari, M. O. Ansari, B. K. Min, J. Lee and M. H. Cho, *J. Phys. Chem. C*, 2014, DOI: 10.1021/jp500933t.
44 V. Eskizeybek, F. Sari, H. Gülce, A. Gülce, A. Avcı, *Appl. Catal. B-Environ*., 2012, **119-120**, 197.